Supporting Information

Exciton Dynamics in Phthalocyanine Molecular Crystals

Rocco P. Fornari, Juan Aragó,* Alessandro Troisi*

Department of Chemistry and Centre for Scientific Computing, University of Warwick,

Coventry CV4 7AL, UK

1. Modified force field with optimized π bond orders

In order to ensure that the electronic structure of the frontier orbitals, which depends largely on the geometry of the aromatic backbone of the H_2-OBPc molecule, remains consistent along the molecular dynamics (MD) simulation, the standard MM3 force field[1] has been modified as follows. The bond orders of the bonds involved in the π-system have been i) optimized to match the equilibrium bond lengths obtained from a quantum chemistry (QC) geometry optimization and ii) kept constant during the MD simulation, with the additional advantage of speeding up the simulation. The optimization was performed as follows. The first guess for the bond orders B, and the corresponding bond lengths L, were obtained from the Tinker *optimize* program[2] using the standard MM3 force field. The reference bond lengths L_{ref} were obtained from a geometry optimization performed at the LC-ωPBE/6-31G** level of theory. Since the bond lengths depend linearly on the bond orders ($L = L_0 + mB$), we obtained the proportionality constant m and the intercept L_0 from a linear fitting. The C-C and C-N aromatic bonds were fitted separately as they have different values of m and L_0. The corrected bond orders were then calculated for each set of bonds as $B_{corr} = B + (L_{ref} - L) / m$ and used to obtain a new set of bond lengths from the force field. The procedure was repeated until the root mean square of the length difference, $\sqrt{\left\langle \left(L_{ref} - L \right)^2 \right\rangle}$, fell below 0.01 Å. The largest length difference at convergence was $7.2 \cdot 10^{-3}$ Å.

2. Excitation energies of the H_2-OBPc monomer and excitonic couplings in H_2-OBPc dimers

Figure S1 displays the excitation energies, oscillator strengths and description of the first two singlet excited states of the H_2-OBPc molecule at the crystal structure as well as the frontier molecular orbitals involved in the electronic transitions and the orientation of the transition dipole moments for S_1 and S_2 computed at the LC-ωPBE/6-31G** level. The first two excited states S_1 and S_2 calculated at 1.73 and 1.74 eV can be described as one-electron promotions from the highest occupied molecular orbital (HOMO) to the lowest unoccupied molecular orbitals (LUMO and LUMO+1). The S_1 and S_2 states present transition dipole moments polarized in almost perpendicular directions with similar oscillator strengths.

a)

State	ΔE (eV)	Oscillator strength	Main contributions (c^2)
S_1	1.73	0.46	HOMO → LUMO (0.13) HOMO → LUMO+1 (0.77)
S_2	1.74	0.49	HOMO → LUMO (0.80) HOMO → LUMO+1 (0.12)

b)

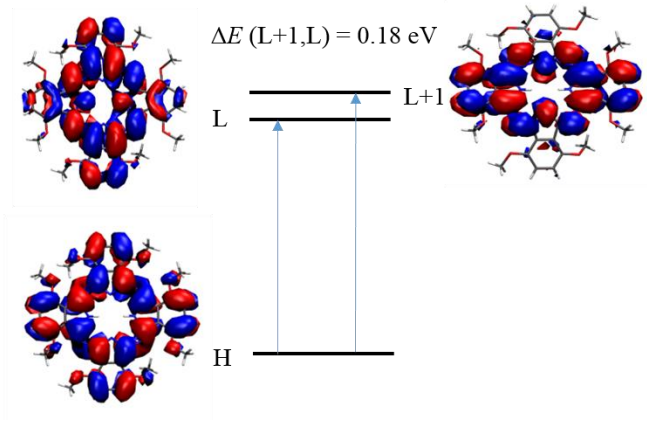

c)

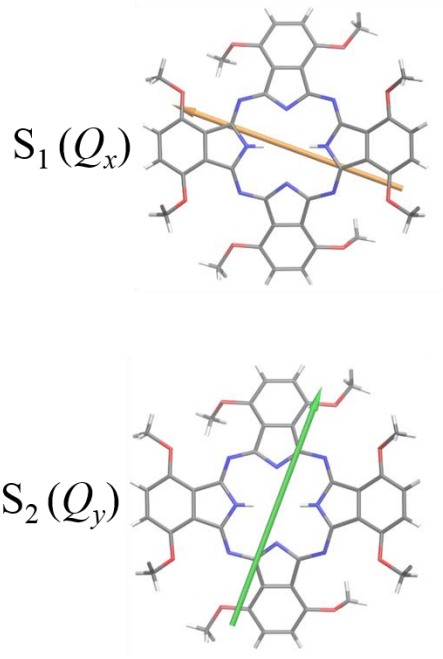

Figure S1. Excitation energies, oscillator strength and description of the first two excited states of H_2-OBPc (a), molecular orbitals involved in the first two excited states (b), and orientation of the transition dipole moments for the H_2-OBPc monomer (c). H and L denote HOMO and LUMO. Level of theory LC-ωPBE/6-31G**.

In the H_2-OBPc dimers, the diabatic Hamiltonian (obtained with the method described in the main text, section Methods 1) has the following structure:

$$\mathbf{H^D} = \begin{bmatrix} E_1^{D,1} & J_{1xy} & J_{xx} & J_{xy} \\ & E_2^{D,1} & J_{yx} & J_{yy} \\ & & E_1^{D,2} & J_{2xy} \\ & & & E_2^{D,2} \end{bmatrix} \quad (1)$$

where $E_i^{D,j}$ denotes the diabatic energy of the excited state i located on molecule j. J_{1xy} and J_{2xy} are the intramolecular excitonic couplings between the first two excited states (Q_x and Q_y) located on the same molecule, whereas J_{xx}, J_{xy}, J_{yx}, and J_{yy} are the intermolecular couplings (those that stem from the interactions between the first two excited states Q_x and Q_y localized on different molecules). In principle, the intramolecular couplings should be close to zero since the Q_x and Q_y states located on the same molecule present almost perpendicular transition dipole moments.

Figure S2 shows a comparison between the intermolecular excitonic couplings computed with the 3-21G* and 6-31G** basis sets as a function of the intermolecular distance between the planes formed by the isoindole groups. Although the difference between the excitonic couplings computed with the small 3-21G* and the larger 6-31G** basis sets is significant, the distance dependence is qualitatively the same. There is a systematic error associated with the smaller basis set which is expected to have little effect on the values of the couplings averaged over the MD simulation and does not justify the large computational cost of performing ~500 calculations at the TDDFT/LC-ωPBE/6-31G** level. In principle, the couplings obtained with the 3-21G* basis set could be corrected using a scaling factor obtained from a fitting of the data shown in Figure S2, but the difference in the values of the excitonic couplings is not expected to affect significantly the findings of this work.

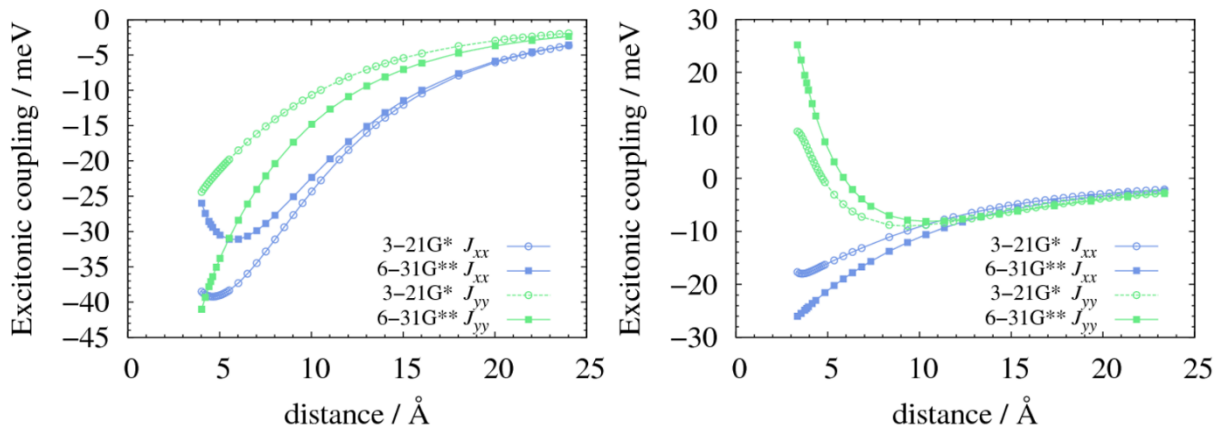

Figure S2. Intermolecular excitonic couplings as a function of the intermolecular π-π stacking distance between the planes formed by the isoindole rings for dimers A (left) and B (right) at the TDDFT/LC-ωPBE level with the 3-21G* and 6-31G** basis sets.

Figure S3 collects the excitonic couplings computed for three intercolumnar dimers (C, D and E). The three dimers exhibit in general excitonic couplings smaller than those found for intracolumnar dimers (A and B). It is therefore expected that the exciton transport is more important along the 1D crystal packing and intercolumnar dimers have not been taken into account.

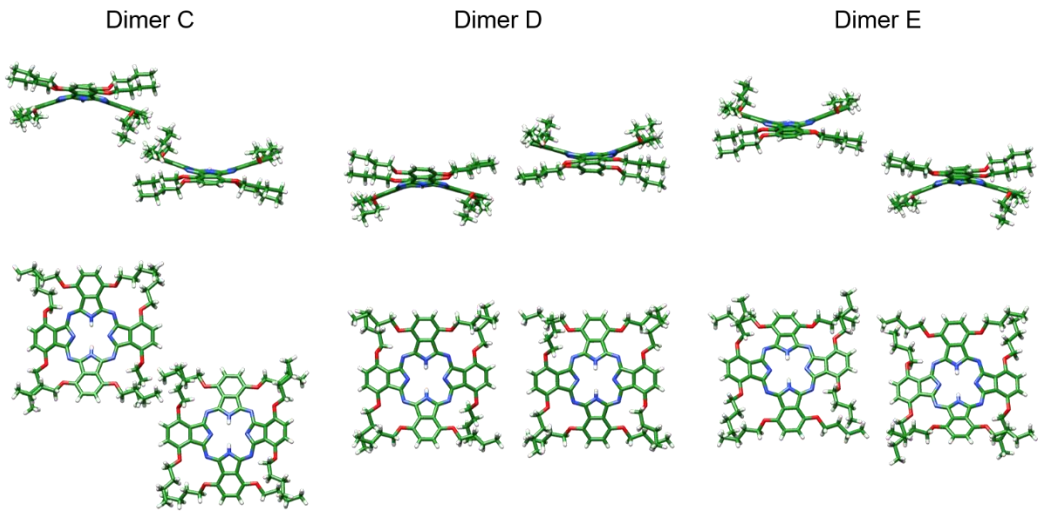

Dimer	J_{xx}	J_{xy}	J_{yx}	J_{yy}
A	−38.51	−8.77	−8.71	−24.40
B	−17.68	18.12	18.12	8.86
C	9.23	7.06	7.06	−4.23
D	13.96	−2.65	−2.65	−6.21
E	7.18	−1.64	−1.65	−5.88

Figure S3. Molecular structure of the three intercolumnnar dimers (C, D and E) with the closest intermolecular contacts and comparison of the excitonic couplings (meV) between intracolumnar dimers A and B and the intercolumnar dimers C, D, and E computed at LC-ωPBE/3-21G*.

Figure S4 shows the comparison between the total intermolecular excitonic couplings (obtained from the diabatization scheme) and the purely Coulombic excitonic couplings as a function of the intermolecular distance between the planes formed by the isoindole groups. The purely Coulombic excitonic couplings are computed by using the following expression (in atomic units):

$$J_{rs}^{C} = \sum_{i}\sum_{j}\frac{q_{i,r}^{A} q_{j,s}^{B}}{R_{ij}} \qquad (2)$$

where $q_{i,r}^{A}$ and $q_{j,s}^{B}$ are the atomic transition charges (ATCs) associated with the *r*-th and *s*-th electronic excitations of the individual molecules A and B (*r* and *s* are the Q_x and Q_y excited states in this case). R_{ij} is the distance between the atoms. At long intermolecular distances the total excitonic couplings are, as expected, almost identical to the Coulombic couplings computed from the ATCs of the two excited states of the isolated molecules. Only at short/intermediate intermolecular distances, the non-Coulombic short-range effects might become important.

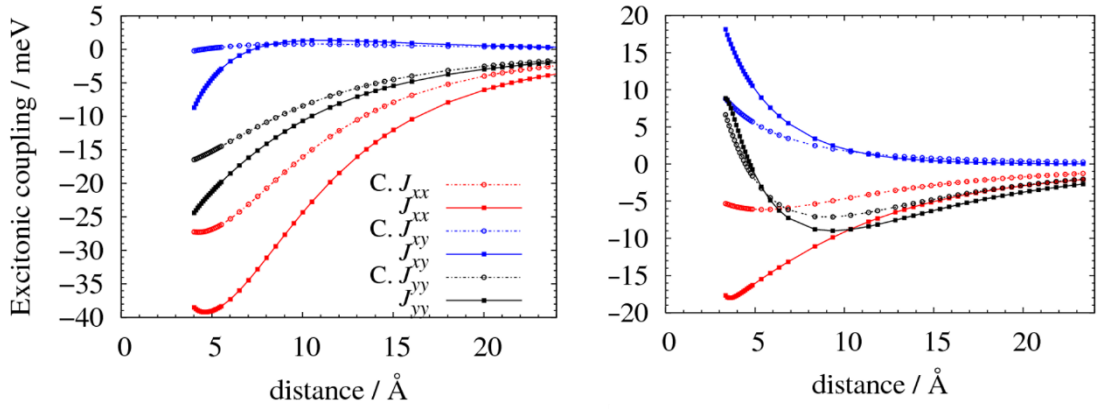

Figure S4. Total (solid) and Coulombic (dotted) excitonic couplings as a function of the intermolecular π-π stacking distance between the planes formed by the isoindole rings for dimers A and B at the LC-ωPBE/3-21G* level.

Figure S5 displays the intramolecular excitonic couplings (J_{1xy} and J_{2xy}) as a function of the intermolecular π-π stacking distance between the planes formed by the isoindole rings for dimers A and B at the LC-ωPBE/3-21G* level. At short intermolecular distances it is evident that these J_{1xy} and J_{2xy} couplings increase when the molecules become closer. This can be explained because we are using quantum chemical calculations in dimer systems for the diabatization process and, thus, excited states localized on the same molecule may be now

mixed owing to the presence of the other molecule (i.e., an electrostatic perturbation). To study this in more detail, we have computed the excitonic couplings between the first two excited states in a model that consists of a dimer of a H_2-OBPc molecule and the interacting isoindole group of the other molecule (Figure S6). Now, we only focus on the excitonic coupling between the first two excited states localized on the phthalocyanine molecule. The excited states in the isoindole group are found to be higher in energy. The intramolecular couplings J_{1xy} are found to be 1.89 and 12.36 meV for dimer A and B, respectively. These values are similar to those computed with the whole diabatization 4 × 4 scheme. This clearly confirms that these non-vanishing intramolecular couplings are not an artifact of the diabatization process.

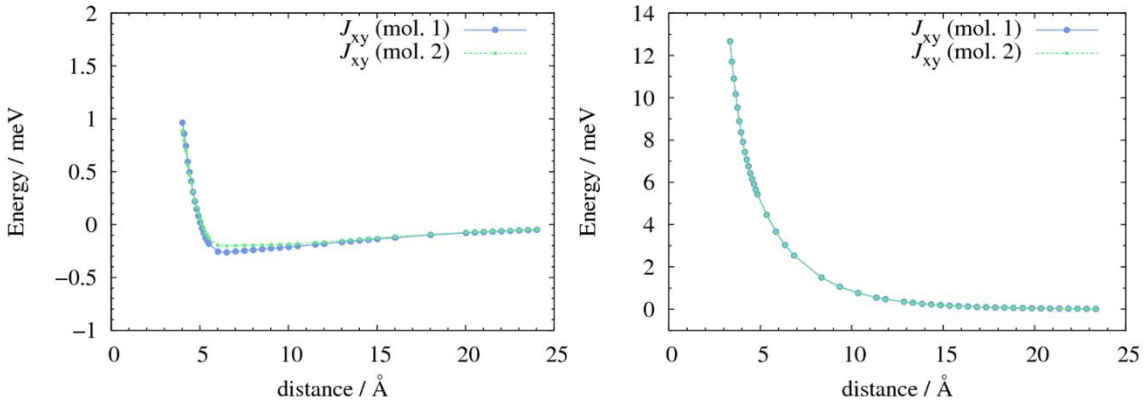

Figure S5. Intramolecular excitonic couplings (J_{1xy} and J_{2xy}) as a function of the intermolecular π-π stacking distance between the planes formed by the isoindole rings for dimers A and B at the LC-ωPBE/3-21G* level.

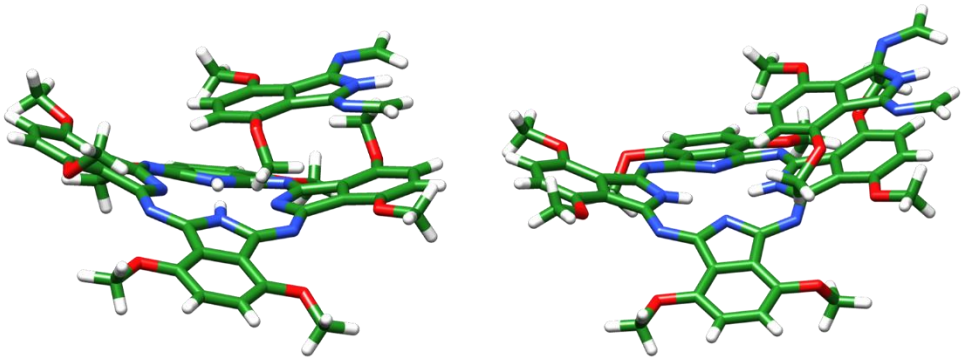

Figure S6. Molecular structure of the model dimers used to analyse the intramolecular J_{1xy} and J_{2xy} excitonic couplings.

3. Fluctuations of the excitonic couplings

The relationship between the thermal motions of the molecules and the fluctuations of the excitonic couplings has been investigated by computing the Fourier transformation of the autocorrelation function $\langle \delta J(0)\delta J(t) \rangle$ for each coupling (Figure S7), using the same procedure as described in ref. 3. The resulting spectra, reported in Figure S8, show that low frequency vibrations below 100 cm^{-1} contribute significantly to the fluctuations of all couplings. Most of the couplings also show a significant peak in the frequency spectrum just above 300 cm^{-1}, which is most likely due to an intramolecular mode. However, as shown in Figure S7, the amplitude of the fluctuations of the autocorrelation function induced by this high-frequency mode is small compared to the amplitude of the low-frequency beating. Therefore, in order to keep the model Hamiltonian for the exciton dynamics (eq. 1 in the main text) more simple, it is more convenient to assume that the couplings are modulated by only one effective low frequency intermolecular mode, while the 300 cm^{-1} mode can be neglected for the purpose of this work. The effective frequency for each coupling in each dimer was determined as the average frequency (weighted on the spectral density) in the range 0–100 cm^{-1}. By averaging over all couplings in both dimers we obtained an effective frequency of 40 cm^{-1}.

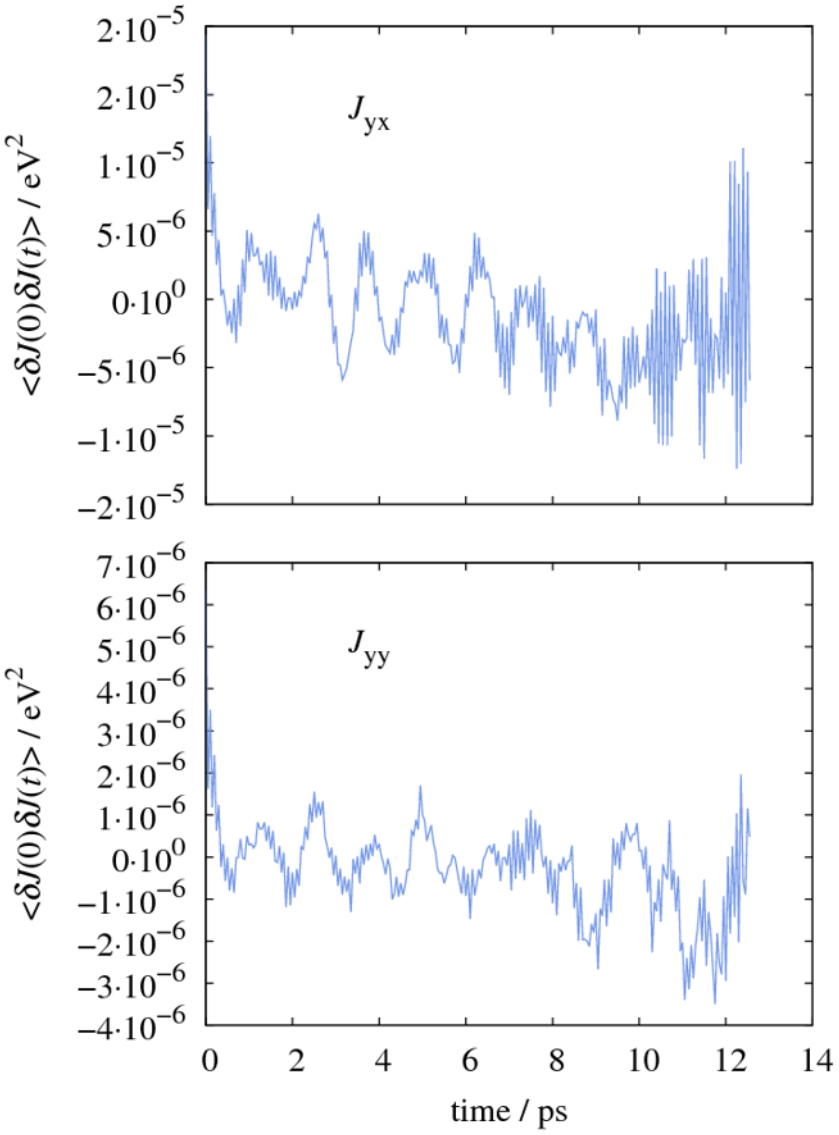

Figure S7. Time evolution of the autocorrelation function of two couplings of dimer A.

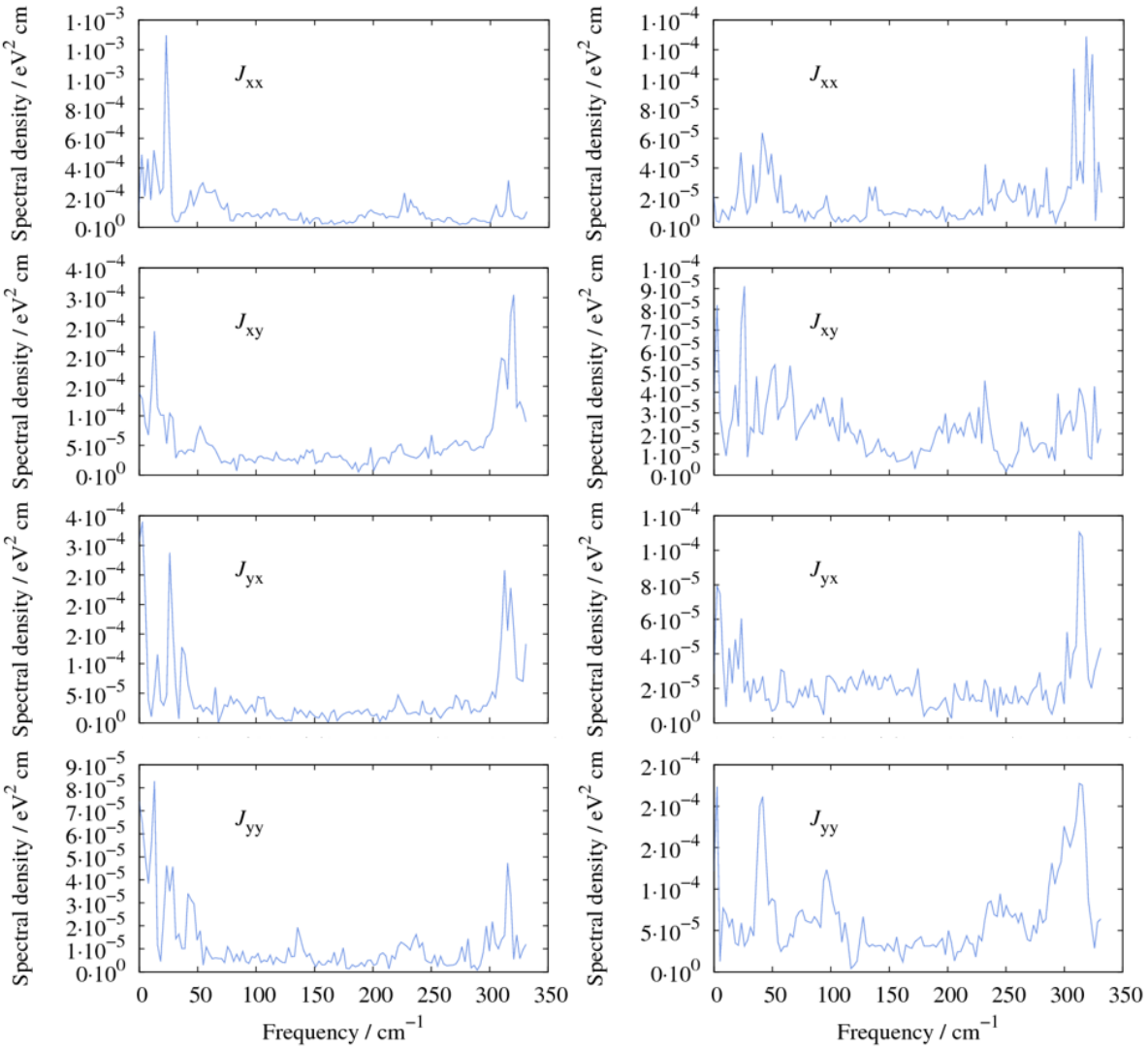

Figure S8. Fourier transformation of the autocorrelation function of the four intermolecular excitonic couplings in dimers A (left) and B (right). Data obtained from the MD simulation at 300 K (see Figure 3, main text).

In order to investigate possible correlations between the couplings of dimers A and B, which share one molecule as they are consecutive in the 1D stack, we computed the statistical correlation factor, $cor\left(J_{ij}^{A}, J_{ij}^{B}\right) = \dfrac{\left\langle J_{ij}^{A} J_{ij}^{B} \right\rangle - \left\langle J_{ij}^{A} \right\rangle \left\langle J_{ij}^{B} \right\rangle}{\sigma_{J_{ij}^{A}} \sigma_{J_{ij}^{B}}}$, for each couple of intermolecular couplings, where $\langle\ \rangle$ denotes averaging over the MD simulation. The results are collected in

Table S1 and show that none of the correlations is particularly strong. The largest value is found for the couplings J_{xx} and J_{xy}. The values of these couplings for all MD snapshots, reported in Figure S9, suggest that there is no significant correlation between them. We can therefore safely assume that all couplings in dimers A and B are uncorrelated.

Table S1. Correlations $cor\left(J_{ij}^{A}, J_{ij}^{B}\right)$ between the excitonic couplings in dimers A and B.

$cor\left(J_{ij}^{A}, J_{ij}^{B}\right)$	J_{xx}	J_{xy}	J_{yx}	J_{yy}
J_{xx}	−0.034	−0.248	0.007	0.038
J_{xy}		0.185	−0.024	−0.208
J_{yx}			−0.088	0.020
J_{yy}				−0.116

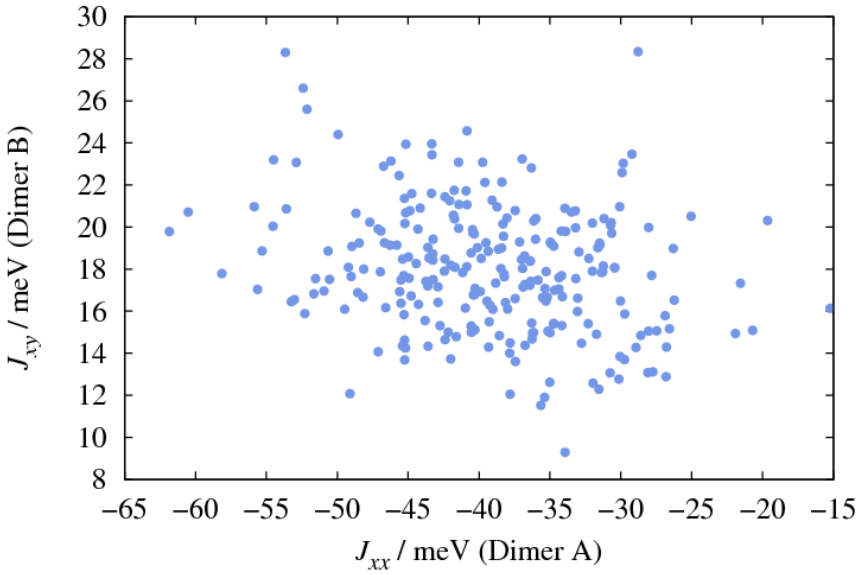

Figure S9. Values of the intermolecular couplings J_{xx} and J_{xy} in dimers A and B for all 250 snapshots of the MD simulation.

4. Local exciton-phonon couplings and adiabatic potential energy surfaces for the excitation energy transfer.

Figure S10 represents the potential energy surfaces for the ground state (S_0) and first excited state (S_1) of the two molecules (labeled as 1 and 2) involved in the exciton transfer process. The intramolecular reorganization energy consists of two terms related to the geometry relaxation energies of one molecule going from the fully relaxed ground state to the electronic excited state (Figure S10, left) and a neighboring molecule evolving in the opposite way (Figure S10, right),

$$\lambda = \lambda_{S_1}^{(1)} + \lambda_{S_0}^{(2)} \tag{3}$$

$$\lambda_{S_1}^{(1)} = E^{(S_1)}(M1) - E^{(S_1)}(M1^*) \tag{4}$$

$$\lambda_{S_0}^{(2)} = E^{(S_0)}(M2^*) - E^{(S_0)}(M2) \tag{5}$$

Here, $E^{(S_1)}(M1)$ and $E^{(S_1)}(M1^*)$ for molecule 1 are the energies of the first excited state at the equilibrium ground state geometry and the relaxed excited state geometry, respectively, and $E^{(S_0)}(M2^*)$ and $E^{(S_0)}(M2)$ for molecule 2 are, accordingly, the energies of the ground state at the relaxed excited state geometry and at the equilibrium ground state geometry. On the other hand, $\lambda_{S_1}^{(1)}$ and $\lambda_{S_0}^{(2)}$ can also be expressed as the sum of the contributions of each vibrational mode; for instance $\lambda_{S_1}^{(1)} = \sum_k \hbar\omega_k S_k$ where S_k denotes the Huang-Rhys factor for the normal mode *k* (Figure S10). The calculation of each S_k is carefully explained in ref. 4.

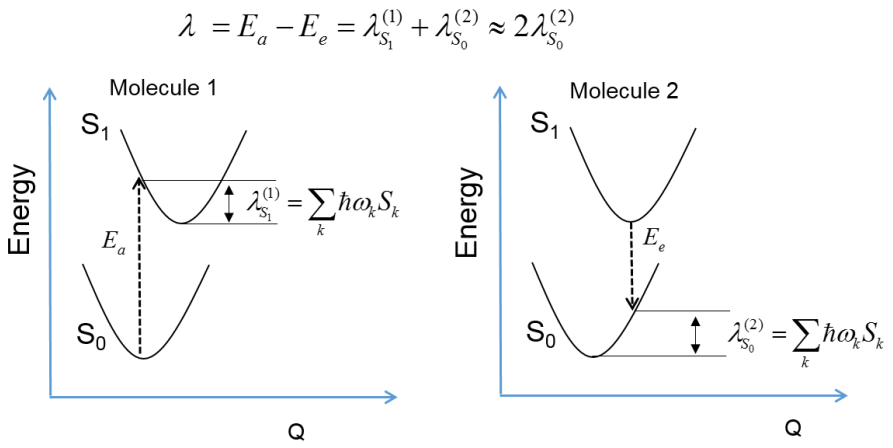

Figure S10. Scheme of the potential energy surfaces of the ground state and the first excited state in the monomeric representation for two molecules involved in the exciton transfer process. $\lambda_{S_1}^{(1)}$ and $\lambda_{S_0}^{(2)}$ are the two contributions to the total reorganization energy (λ).

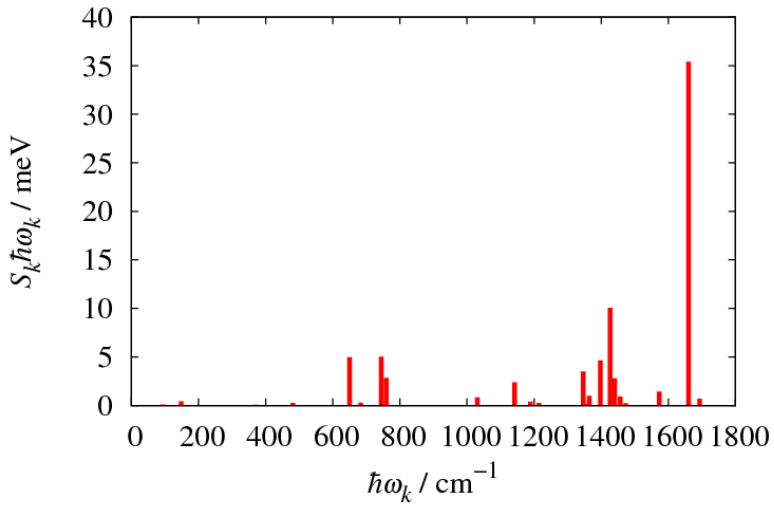

Figure S11. Individual relaxation energy contribution ($\hbar\omega_k S_k$) for each normal mode ($\hbar\omega_k$) in the second singlet excited state S_2.

Figure S12 shows a representation of the diabatic and adiabatic potential energy surfaces (PES) computed from the average exciton coupling for dimer B ($|\langle J_{xx}\rangle|$ = 18.07 meV) and the total reorganization energy (λ = 110.89 meV). Two well-defined minima are found separated by an energy barrier (12.60 meV) much higher than that obtained for dimer A (Figure 4, main text). Nevertheless, if we take into account the thermal energy k_BT (25.85 meV) and the zero point energy, $E_{ZPE} = 1/2\hbar\omega_{eff} = 72.16$ meV, it is evident that both k_BT and E_{ZPE} are enough to overcome the energy barrier between the two adiabatic minima. In this context, it seems difficult to be able to assume an incoherent regime for the exciton transport and, therefore, the use of a nonadiabatic transfer rate.

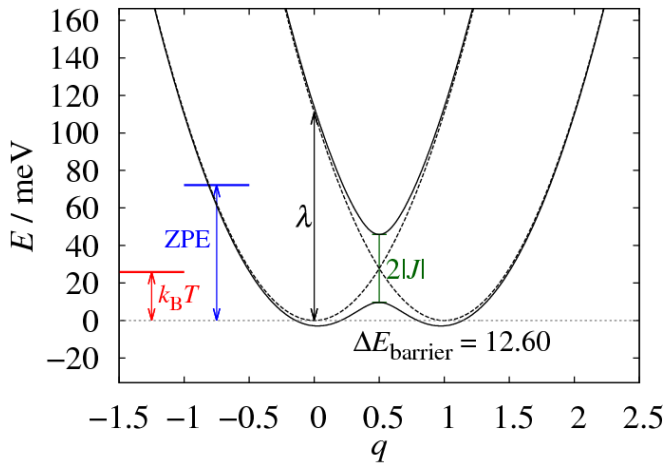

Figure S12. Representation of the diabatic (dotted lines) and adiabatic (solid lines) potential energy surfaces computed with the average exciton coupling for dimer B ($|\langle J_{xx}\rangle|$) and the total reorganization energy previously computed. The thermal energy (k_BT) and zero point energy (E_{ZPE}) are also given.

Figure S13 shows the time evolution of the exciton wavefunction and temperature averaged squared displacement versus time using the parameters of Table 2 but where only a single excited state per site (Q_x) is included in the model. From this simpler model, we have obtained a smaller exciton diffusion coefficient (D = 0.095 cm^2 s^{-1}) in comparison with the complete model (two electronic excited states per site) in the main text. The comparison between both models clearly reveals that the incorporation of the two electronic excited states close in energy (Q_x and Q_y) gives rise to an enhanced exciton transport pathway.

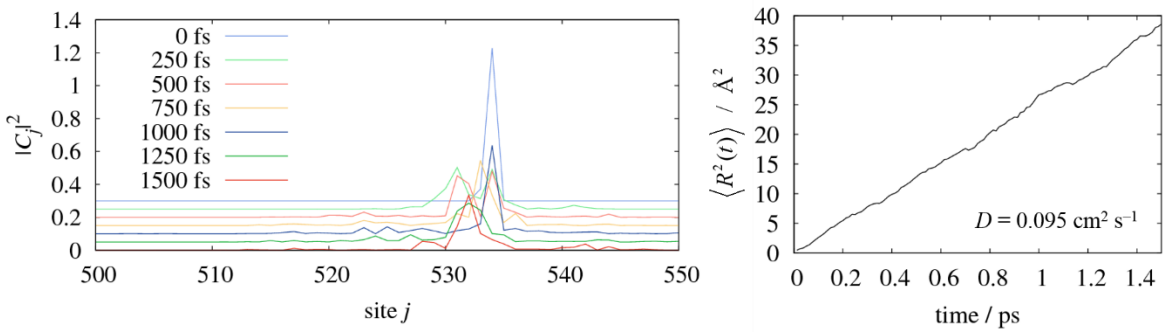

Figure S13. Time evolution of the exciton wavefunction evaluated from the model Hamiltonian (left) and plot of the temperature averaged square displacement $\langle R^2(t) \rangle$ (in Å^2) versus time using the parameters of Table 2 (right). Only a single excited state per site is considered in the model Hamiltonian

(1) a) Allinger, N. L.; Yuh, Y. H.; Lii, J.-H. Molecular Mechanics. The MM3 Force Field for Hydrocarbons. 1. *J. Am. Chem. Soc.* **1989**, *111*, 8551–8566. b) Lii, J.-H.; Allinger, N. L. Molecular Mechanics. The MM3 Force Field for Hydrocarbons. 2. Vibrational Frequencies and Thermodynamics. *J. Am. Chem. Soc.*, **1989**, *111*, 8566–8575. c) Lii, J.-H.; Allinger, N. L. Molecular Mechanics. The MM3 Force Field for Hydrocarbons. 3. The van der Waals' Potentials and Crystal Data for Aliphatic and Aromatic Hydrocarbons. *J. Am. Chem. Soc.* **1989**, *111*, 8576–8582.

(2) Ponder, J. W.; Richards, F. M. An Efficient Newton-like Method for Molecular Mechanics Energy Minimization of Large Molecules. *J. Comput. Chem.* **1987**, *8* (7), 1016–1024.

(3) Aragó, J.; Troisi, A. Dynamics of the Excitonic Coupling in Organic Crystals. *Phys. Rev. Lett.* **2015**, *114* (2), 026402.

(4) Malagoli, M.; Coropceanu, V.; da Silva Filho, D. A.; Brédas, J. L. A Multimode Analysis of the Gas-Phase Photoelectron Spectra in Oligoacenes. *J. Chem. Phys.* **2004**, *120*, 7490.